Available online at www.sciencedirect.com

ScienceDirect

Advances in Space Research 73 (2024) 992–1005

ADVANCES IN SPACE RESEARCH
(a COSPAR publication)

www.elsevier.com/locate/asr

Trajectory planning of stratospheric airship for station-keeping mission based on improved rapidly exploring random tree

Qin-chuan Luo [a], Kang-wen Sun [a], Tian Chen [b,*], Yi-fei Zhang [c,*], Ze-wei Zheng [d,*]

[a] *School of Aeronautic Science and Engineering, Beihang University, Beijing 100191, China*
[b] *Institute of Unmanned System, Beihang University, Beijing 100191, China*
[c] *School of Electronic and Information Engineering, Beihang University, Beijing 100191, China*
[d] *School of Automation Science and Electrical Engineering, Beihang University, Beijing 100191, China*

Received 7 March 2023; received in revised form 23 July 2023; accepted 4 October 2023
Available online 10 October 2023

Abstract

The station-keeping mission is one of the common missions of stratospheric airships. Its movement is sensitive to wind due to the large size and low airspeed of stratospheric airships. When the wind speed exceeds the maximum airspeed of the airship, the airship may fly out of the given mission region. Therefore, station-keeping trajectory planning is a new trajectory planning problem that has never existed before. A rapidly exploring random tree algorithm for station-keeping(RRT-SK) is proposed to solve the trajectory planning problem under multiple constraints of the airship, and an artificial potential field method (APF) considering wind field and relative position is designed as the objective function of the RRT-SK algorithm, both of which form the RRT-SK strategy used for the stratospheric airship station-keeping trajectory planning under multiple constraints. A multidisciplinary model is developed to simulate multiple constraints on the airship flight, including the energy model, thermal model, propulsion model, and kinematic model. The performance of the RRT-SK strategy is demonstrated in this multidisciplinary model with real wind fields. The results show that the multi-constrained station-keeping problem can be solved by the RRT-SK strategy. Compared with the conventional strategy, the RRT-SK strategy can improve the success rate of the airship's 24-h stationing flight and well cope with the impact of wind field changes and stationing area changes. Moreover, the RRT-SK strategy has better advantages in actual long-duration use.

Keywords: Stratospheric airship; Trajectory planning; Wind potential energy; Location potential energy; Rapidly exploring random tree(RRT)

1. Introduction

In recent years, there has been a growing interest in stratospheric airships. As high-altitude platforms, stratospheric airships can remain at an altitude of 20 km for weeks, months, or even years. Therefore, stratospheric airships have great potential for applications in areas that require long periods of time to remain stationary, such as communications relay, meteorological research, and Earth observation (Colozza and Dolce, 2003; Du et al., 2019b).

Compared to conventional air vehicles, stratospheric airships are one of the few aircraft that require station-keeping trajectory planning. Stratospheric airships rely on buoyancy to maintain their altitude, and in order to obtain a larger carrying capacity, stratospheric airships require a large capsule to store helium, resulting in a large windward area and a high drag coefficient characteristic, whose motion is susceptible to wind (Mueller et al., 2004; d'Oliveira and Melo, 2016). Therefore, there is an urgent

* Corresponding authors.
E-mail addresses: qinchuan@buaa.edu.cn (Q.-c. Luo), sunkw100@buaa.edu.cn (K.-w. Sun), chen_tian@buaa.edu.cn (T. Chen), zyifei@buaa.edu.cn (Y.-f. Zhang), zeweizheng@buaa.edu.cn (Z.-w. Zheng).

https://doi.org/10.1016/j.asr.2023.10.002
0273-1177/

need for trajectory planning to avoid the change of position of the airship due to the wind influence.

Trajectory planning for the airship is a multi-constrained optimization problem, limited by location constraints, and also by energy and temperature constraints. The airship are usually solar-powered, and the energy generated in a day is limited, and the airships need to plan a proper trajectory to ensure that the energy will not be exhausted. The pressure differential in the airship's capsule is positively correlated with temperature. As the sun heats the capsule during the day, the capsule pressure differential rises with its temperature, and the risk of capsule explosion increases with an excessive capsule pressure differential. The main method to reduce the capsule temperature is to accelerate air convection by maintaining a high airspeed (Alam et al., 2023). Therefore, trajectory planning strategies designed for the stratospheric airship must be able to solve the multi-constraint planning problem.

The stratospheric airship must continue to move forward in order to withstand the wind and dissipate the heat when it is used for the station-keeping mission. As a result, a trajectory planning strategy is required for the station-keeping mission. For this scene, there are few algorithms exist. Regarding energy consumption, Zhang and Shan, respectively, proposed a station-keeping strategy in one dimension (Zhang et al., 2020; Shan et al., 2020). Researchers from Google conducted a height adjustment analysis of the station-keeping problem based on unpowered balloons (Bellemare et al., 2020). Zhang proposes a solution to solve the regional coverage problem based on multiple stratospheric airships, but without considering the effects of strong winds (Zhang et al., 2022a). Because in practice the airship's trajectory needs to be adjusted in accordance with the predicted wind field, it is necessary to develop a trajectory planning strategy for the station-keeping mission in two-dimensional space.

Researchers have proposed many kinds of trajectory planning algorithms for different problems. In the past, the optimal path was considered as the shortest path, and the determined algorithm was used to find the shortest path (Souissi et al., 2013). As the problem evolves, the optimal path is now associated with energy consumption and region avoidance. To solve these complex problems, researchers have changed from using deterministic algorithms to using uncertain algorithms (Aggarwal and Kumar, 2020). The typical algorithms include Random sampling search algorithms, such as probabilistic road map (Liu et al., 2023); Best search algorithm, such as Dijkstra's algorithms, A*, D* (Bai et al., 2023; Wang et al., 2023; Jin et al., 2023); Visibility Graph (Ou et al., 2023); bio-inspired planning algorithms (Zhang et al., 2022b). Nevertheless, almost all algorithms do not guarantee fast convergence, let alone real-time planning in stratosphere wind fields with rapid change. Among all the path planning algorithms, Rapidly-exploring Random Tree (RRT) proposed by LaValle (LaValle et al., 1998), is proved to be fast convergence and computational efficient, thus enabling online implementations. RRT algorithm is a random sampling algorithm for state space. This method is probabilistic complete and non-optimal. Through collision detection of sampling points, it avoids the large amount of calculation caused by the accurate modeling of space, and can effectively solve the path planning problem of high-dimensional space and complex constraints (Zhao et al., 2023).

Since the wind significantly affects the airships' motion, station-keeping mission trajectory planning is a unique problem to take into account for the airship. Because almost all of the aforementioned algorithms are created for point-to-point scenarios, the artificial potential field method (APF) is introduced as a computationally effective guidance scheme in this paper to address the issue of no termination point. The artificial potential field method (APF) (Sigurd and How, 2003; Kitamura et al., 1995) is commonly used in local path planning. The concept of "field" in conventional mechanics is introduced into this method. It is assumed that the vehicle moves under this virtual force field, but there is a limitation in that it is easy to fall into local minima. Combined with the randomness of the RRT, the APF local minimum problem can be avoided. Based on the artificial potential field method, the station-keeping potential energy is introduced to evaluate the station-keeping ability of the stratospheric airship. With the potential energy of the airship as the objective function, the trajectory that meets the requirements of the station-keeping mission can be obtained by the strategy this paper proposed.

The main contributions of this paper are as follows: First, the station-keeping mission trajectory planning problem of the stratospheric airship is firstly investigated in two-dimensional space, considering multiple constraints during the airship flight, such as energy constraints and thermal constraints, to ensure the feasibility of the trajectory. Second, a new trajectory planning strategy is proposed for solving the no-endpoint trajectory planning problem, which will be met in the station-keeping mission. Compared with (Zhang et al., 2020; Shan et al., 2020; Bellemare et al., 2020), the RRT algorithm is properly modified in order to solve the endpoint-free problem, and the APF method is introduced as the objective function of the RRT algorithm to bias the random sampling to the optimal solution. Later on, potential energy functions are designed for the airship station-keeping mission, including position potential energy and wind field potential energy, which together with the airship battery energy constitute the airship stationing potential that can be used to evaluate the optimal position of the airship.

The structure of this paper is as follows: In Section 2, system modeling and problem formulation are presented. In Section 3, rapidly exploring random trees for station-keeping(RRT-SK) strategy is introduced along with integration of the APF. In Section 4, a multidisciplinary model is established as an example to simulate the multiple constraints encountered when planning the trajectory of the airship. In Section 5, simulations are performed to demonstrate the effectiveness of the proposed strategy. Finally, Conclusions are provided in Section 6.

2. Problem statement

2.1. System modeling

In this brief, the airship is modeled as a rigid body, thus the aeroelastic effects of the airship can be ignored.

Firstly, as shown in Fig. 1, an inertial coordinate system is established. The origin O_n is located anywhere in the same horizontal plane as the airship, and O_nx_n-axis and O_ny_n-axis point to north and east respectively.

Unlike conventional air vehicles, the balance of the stratospheric airship is provided by buoyancy (Khoury, 2012), which results in a natural stabilizing moment about the roll axis and pitch axis. Unless gas leaks and wind effects change the altitude of the airship, the balance of gravity and buoyancy keeps the altitude of the airship at a fixed value for a long time. The following assumptions are made:

Assumption 2.1. Changes in roll and pitch angle are little enough to be ignored.

Assumption 2.2. The airship altitude change is ignored in this research.

Based on the above assumptions, the simplified kinematic equations of the airship can be expressed as (Wang et al., 2021; Zhang et al., 2022a)

$$\begin{cases} \dot{x} = v\cos\gamma + w_x \\ \dot{y} = v\cos\gamma + w_y \end{cases} \tag{1}$$

where $[x, y]^T$ denotes the vector of position of the airship, v is the airspeed of the airship, $\gamma \in [-\pi/2, \pi/2]$ is the yaw angle between the airspeed and the positive direction of O_nx_n-axis, w_x and w_y are the components of the wind.

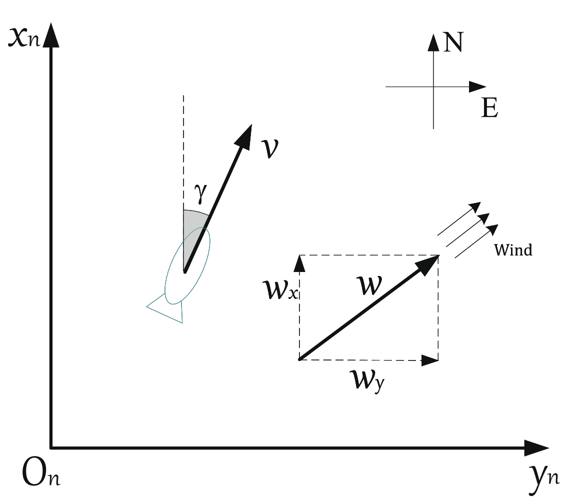

Fig. 1. The reference coordinate system.

2.2. Problem formulation

Let $x(t) = (\xi, \delta) \in \mathbb{X}$ be the measurable state of the system, where $\delta \in \mathbb{X}^n$ is other n states related to the airship trajectory planning. and $u = (v, \gamma)^T \in \mathbb{U}$ be a control input in the set $\mathbb{U}$ of admissible controls. Then, the differential system can be written as

$$\dot{\boldsymbol{x}} = \boldsymbol{f}(\boldsymbol{x}, \boldsymbol{u}, \boldsymbol{w}) \tag{2}$$

where $\boldsymbol{f}$ is the vehicle system model.

$\mathbb{X} = \mathbb{R}^{3+n}$ is the state space. It is divided into two subsets. Let $\mathbb{X}_{free}$ be the set of admissible states. $\mathbb{X}_{obs} = \mathbb{X}/\mathbb{X}_{free}$ is defined as the obstacle state needs to be avoided. The initial state of the system is $x_{init} \in \mathbb{X}_{free}$.

The path planning algorithm is given a rendezvous set $\mathbb{X}_{goal} \in \mathbb{X}_{free}$. To achieve its mission, the airship has to reach $\mathbb{X}_{goal}$ while avoiding obstacles and minimizing a performance criterion J defined as

$$J(t_0, t_f, \boldsymbol{u}) = \int_{t_0}^{t_f} f^0(\boldsymbol{x}(t), \boldsymbol{u}(t), \boldsymbol{w}(t))\, dt + k(\boldsymbol{x}(t_f)) \tag{3}$$

where $f^0 : \mathbb{R}^3 \times \mathbb{R}^2 \times \mathbb{R}^2 \to \mathbb{R}$ and k: $\mathbb{R}^3 \to \mathbb{R}$ are C^1.

3. Trajectory planning framework

3.1. Rapidly exploring random trees for station-keeping (RRT-SK)

RRT(see Algorithm 1) is a trajectory planning algorithm whose function is to finally obtain an approximate optimal path connecting the initial point and the endpoint by imitating the growth of the tree after determining the initial point and the end point (Karaman and Frazzoli, 2010; An et al., 2021). The principle of the RRT is described in Algorithm 1. Since the purpose of the station-keeping mission is to stay in a mission area for a long time, the RRT algorithm needs to be improved to make path planning within a mission range rather than reaching a target point. Therefore, the extension method of the node in the RRT algorithm should be changed accordingly. The improved RRT algorithm can be divided into the following steps:

(1) Generate random points in the mission area.

(2) The branch extends from the initial point to the random point. The extension length is determined by the objective function J.

(3) Repeat the step (1)-(2). All nodes of the tree extend to the random points generated in Step3, which is shown in Fig. 2. Besides, Feasibility test is required in process of branch extension.

(4) Merge neighbor nodes into a minimum cost point.

(5) Keep extending the tree until get one or more feasible path with specified step length.

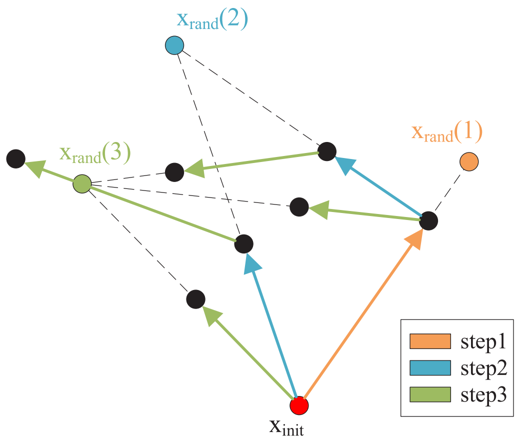

Fig. 2. Example of RRT-SK strategy extension.

Algorithm 1. RRT algorithm

Function
RRT (in :K$\in \mathbb{N}^*, x_{init} \in \mathbb{X}_{free}, \Delta t \in \mathbb{R}^+$, out : G):
  $G \longleftarrow x_{init}$
  cost$(x_{init}) \longleftarrow 0$
  $i = 0$
  repeat
    $x_{rand} \longleftarrow$ random_state$(\mathbb{X}_{free})$
    $x_{nearest} \longleftarrow$ nearest(G, x_{rand})
    $(x_{new}) \longleftarrow$ steer$(x_{nearest}, x_{rand})$
    if collision_free$(x_{nearest}, x_{new})$ **then**
      $G \longleftarrow G \cup \{x_{new}\}$
    end
  until $i++ > K$
  return G

The principle of the RRT-SK as a path planner is described in Algorithm 2. Let G be the exploration tree, E be the set of connection edges of the tree, and cost $((\mathbf{x_1}, \mathbf{x_2}))$ be the minimal cost from $\mathbf{x_1}$ to $\mathbf{x_2}$ according to the objective function J defined in (3). Let cost $(\mathbf{x})$ also be the total cost to arrive at $\mathbf{x}$, that is cost$(\mathbf{x})$ = cost$((\mathbf{x_{init}}, \mathbf{x}))$.

First, the initial state x_{init} is added to the tree G. Then, a state $x_{rand} \in \mathbb{X}_{free}$ is generated randomly. The **RRTSK_extend** extends all nodes of the tree G to $\mathbf{x_{rand}}$ according to a step length d which is defined by **steer** function. In **steer** function, a control input $\mathbf{u}$ is calculated according to some specified algorithm. In this brief, APFs are used as an algorithm to make J minimized.

Then the system model is integrated from $t_{nearest}$ to $t_{nearest} + \Delta T$, to find a new state $\mathbf{x_{new}}$, that is

$$\mathbf{x}_{\text{new}} = \mathbf{x}_{\text{nearest}} + \int_{t_{\text{nearest}}}^{t_{\text{nearest}}+\Delta T} \mathbf{f}(\mathbf{x}, \mathbf{u}) dt \tag{4}$$

A feasibility test (**feasible** function) is performed: if $\mathbf{x_{new}}$ and the path between $\mathbf{x}$ and $\mathbf{x_{new}}$ lie in $\mathbb{X}_{free}$, and control input $\mathbf{u}$ is constraints satisfied, then $\mathbf{x_{new}}$ is added in V.

Next, the RRT-SK algorithm tries to merge neighbor vertices at the same time step. The **near_vertices** function will search the tree G for a set of other vertices with the same time step in a neighborhood $\mathbb{X}_{near} \subset V$ of x_{new}. The state $x_{min} \in \mathbb{X}_{near}$ that minimizes the cost is chosen to be the reserved vertices. Therefore, other vertices in $\mathbb{X}_{near}$ will be replaced by x_{min}, including their state and cost. Besides, the existing connecting edge from the last step to the replaced vertices will be removed.

Algorithm 2. The RRT-SK strategy

Function build_RRT_SK (in :K$\in \mathbb{N}^*$,
 $x_{init} \in \mathbb{X}_{free}, \Delta t \in \mathbb{R}^+$, out : G)
  $G \longleftarrow x_{init}$
  cost$(x_{init}) \longleftarrow 0$
  timestep$(x_{init}) \longleftarrow 0$ $i = 0$
  repeat
    $x_{rand} \leftarrow$random_state$(\mathbb{X}_{free})$
    $G \leftarrow$RRTSK_extend(G, x_{rand})
  until $i++ > K$
  return G

Function RRT_SK_extend (in : G, x_{rand}, out : G_{new})
  $V \longleftarrow G$.Node
  foreach $x(j) \in V$ **do**
    $(x_{j,new}, u) \longleftarrow$ steer(x, x_{rand})
    if feasible$(x(j), x_{new})$ **then**
      $V \longleftarrow V \cup \{x_{new}\}$
      cost$(x_{new}) \longleftarrow$cost$(x(j))$+cost$(x(j), x_{new})$
      timestep$(x_{new}) \longleftarrow$timestep$(x(j))$
  +timestep$(x(j), x_{new})$
      $\mathbb{R}_{near} \longleftarrow$near_vertices$(x_{new}, G)$
      $V \longleftarrow$merge$(V, x_{new}, \mathbb{R}_{near})$
    end
  end
  return G

Function merge (in : $V, x_{new}, \mathbb{R}_{near}$, out : V)
  forall $x_{near} \in \mathbb{R}_{near}$ **do**
    if timestep(x_{near}) =timestep(x_{new})
  and cost(x_{near}) <cost(x_{new}) **then**
      $x_{min} \longleftarrow x_{near}$
    end
  end
  $V \longleftarrow V \setminus (\mathbb{R}_{near} \setminus x_{min})$ **return** V

These steps are repeated until the algorithm reaches K iterations. Thus, the RRT-SK strategy will improve the optimality of the solution over time even after the first solution is found.

Compared with RRT, RRT-SK modifies the following points to meet the needs of station-keeping trajectory planning.

(1) All nodes of tree G are extended during an iteration instead of the nearest node in RRT. Thus allowing more iterations within a set of admissible states rather than reaching a final state.

(2) The step size and control input to the random state is determined by some algorithm rather than a fixed step size in RRT.

(3) Feasibility test during extension instead of collision-free test to take control constraints into account.

(4) Timing information is taken into account for trajectory planning rather than a path planning algorithm like RRT.

(5) The merge function was introduced to solve the data explosion problem.

3.2. State generation using artificial potential fields(APF)

Station-keeping mission is a common mission of the stratospheric airship, which requires the airship to keep floating within the specified distance from the mission point (Du et al., 2019a). The conventional airship trajectory planning strategy is to make the airship fly towards a fixed point by adjusting the heading angle, and the airspeed is a variable that varies according to the distance from the fixed point. This method does not maximize the use of energy. For example, when the wind speed is low during the day, the airship needs very little energy to maintain its position, and the extra energy generated by the solar array will not be stored after the energy storage battery is fully charged, which causes a waste of energy. But at night, energy is often scarce because there is no solar input. Similar to the gravitational potential energy storage strategy of solar aircraft, the airship can fly to the upwind area with extra energy during the day to offset the energy shortage at night. But the airship can not blindly fly to the upwind area without considering the mission boundary.

Based on this, in order to fly to the upwind area while considering the mission boundary, we propose a trajectory planning method based on the airship potential energy. The airship can be considered to have a higher wind potential energy (see Section 3.2.1) in the upwind area. And similar to the wind potential energy, the location potential energy (see Section 3.2.2) can be defined by the airship's location relative to the mission boundary. Together with the energy storage battery of the airship, the airship potential energy function is designed as the objective function to optimize the trajectory, that is

$$E = E_{location} + E_{wind} + E_{battery} \tag{5}$$

where $E_{battery}$ is the energy of storage battery, which can be expressed as

$$E_{battery} = SOC \cdot E_{max} \tag{6}$$

where SOC means state of charge of the battery, and E_{max} denotes the maximum capacity of the battery.

3.2.1. Wind potential energy

As shown in Fig. 3, the potential energy under northerly wind can be understood as follows considering the wind field, if the airship wants to keep the location(point A) unchanged for a period of time Δt, the airspeed is required to be equal to the wind speed, i.e.$V_{airspeed} = V_{wind}$. During this time, energy Q is required to maintain the location of the airship. However, If the airship flew to a specific point B in the upwind zone in advance, even if the airspeed of the airship $V_{airspeed} = 0$, it can still reach point A after Δt. In another word, the energy Q is saved by flying to the upwind area. Energy Q can be regarded as stored in the potential energy of the upwind field, which reduces the airship's energy consumption for wind resistance.

Suppose the airspace center point is the 0 potential energy point, the wind speed is V_{wind}, the wind direction blows from point B to point A, and the wind potential energy at point B is

$$E_{wind} = P_{prop} \cdot \Delta t \tag{7}$$

where P_{prop} is the propulsion power when the airspeed of the airship is equal to the wind speed, which maintains the location of the airship unchanged, expressed as

$$V_{airspeed} = V_{wind} \tag{8}$$

$$P_{prop} = \frac{1}{2}\rho_{air} S_{ref} C_D V_{wind}^3 / (\eta_{prop}\eta_{mot}) \tag{9}$$

where S_{ref} is the cross-sectional area at the maximum shaft diameter, and C_D is the drag coefficient.

Δt in Eq. 7 is the time required for the airship to fly without energy from point B to point A,

$$\Delta t = \frac{y}{V_{wind}} \tag{10}$$

The wind potential energy on a line perpendicular to the wind direction is at the same value. As shown in Fig. 3, the line passing through the origin and perpendicular to the wind direction is the zero potential energy line. Suppose

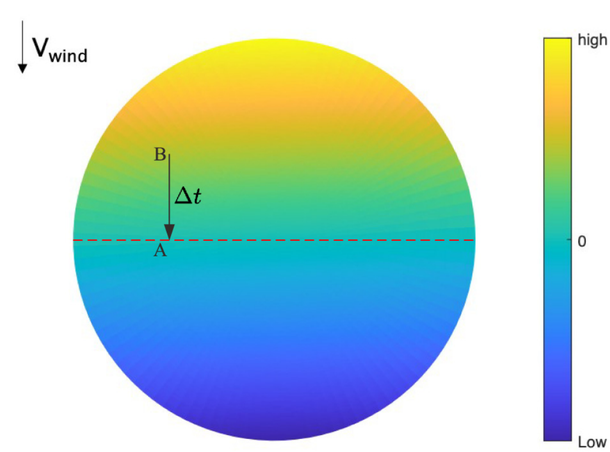

Fig. 3. Wind potential energy.

the direction of the wind field is χ_{wind}, and the potential energy of the wind field at any point (x, y) in the mission area is

$$E_{wind} = \frac{1}{2}\rho_{air}S_{ref}C_D V_{wind}^3/(\eta_{prop}\eta_{mot}) \cdot \frac{x\sin\chi_{wind} + y\cos\chi_{wind}}{V_{wind}} \tag{11}$$

where V_{wind} is wind speed, and χ_{wind} is wind direction.

3.2.2. Location potential energy

Since the stratospheric airship need to stay in a mission area for a long time, suppose its mission area is as shown in Fig. 4, with the center point as the origin, the east direction as the positive direction of the x-axis, and the north direction as the positive direction of the y-axis to establish a coordinate system. The center of the mission area is the best position that can handle the wind in different directions, and a certain amount of energy is needed by the airship to fly to the best place. From the perspective of the potential energy field, this part of the energy is stored in the location potential energy. Suppose the location potential energy of the center is 0, the distance from the center is $R = \sqrt{x^2 + y^2}$, and the location potential energy E_{loc} consumed to fly to the center at the current speed can be expressed by the following

$$E_{loc} = -P_{prop}T_{loc} \tag{12}$$

where P_{prop} is the power of the propulsion system at the current speed, and T_{loc} is the time needed to fly to the center at the current speed. If the current airspeed is $V_{airspeed}$, P_{prop} and T_{loc} can be expressed as

$$P_{prop} = \frac{1}{2}\rho_{air}S_{ref}C_D V_{airspeed}^3/(\eta_{prop}\eta_{mot}) \tag{13}$$

$$T_{loc} = \frac{R}{V_{airspeed}} \tag{14}$$

Thus the positional potential energy can be expressed as

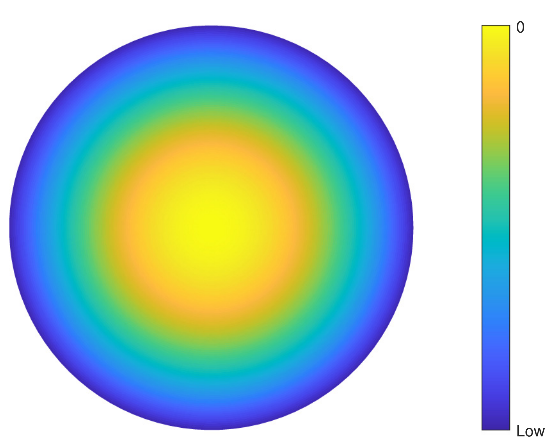

Fig. 4. Location potential energy.

$$E_{loc} = -\frac{1}{2}\rho_{air}S_{ref}C_D V_{airspeed}^3/(\eta_{prop}\eta_{mot}) \cdot \frac{\sqrt{x^2+y^2}}{V_{airspeed}} \tag{15}$$

4. Multidisciplinary modeling

Many constraints need to be considered in the stratospheric airship trajectory planning, including energy constraints, thermal constraints, position constraints, etc. Considering these constraints requires multidisciplinary modeling, including energy modeling, thermal modeling and propulsion power modeling.

4.1. Energy model

4.1.1. Solar radiation model

The types of solar radiation can be divided into direct, scattered, and reflected radiation, which can be assessed from the methods introduced by Iqbal and Muhammad (Iqbal, 2012); Kreith, Frank, and Kreider (Kreith and Kreider, 1978) respectively.

Direct solar irradiance I_D in the stratosphere is expressed as

$$I_D = \tau_h \cdot I_0 \cdot \left(\frac{1 + e_e \cdot \cos(\theta_D)}{1 - e_e^2}\right) \tag{16}$$

where I_0 is the solar radiation intensity constant, which is 1367 W/m^2, e_e is the eccentricity of the Earth's orbit, which is 0.0016708 (Foster and Aglietti, 2010), θ_D is the diurnal angle and can be expressed as

$$\theta_D = 2\pi \cdot (d_n - N_r)/365.24 \tag{17}$$

where d_n is the nth day of the year and N_r is a leap year correction term which can be calculated with

$$N_r = 79.6764 + 0.2422 \cdot (year - 1985) - int\left(\frac{year - 1985}{4}\right) \tag{18}$$

τ_h in Eq. 16 is the atmospheric transparency, and the atmospheric transparency in the stratosphere can be defined by

$$\tau_h = 0.5 \cdot (e^{-0.65 \cdot amr} + e^{-0.95 \cdot amr}) \tag{19}$$

$$amr = \frac{P_H}{P_0} \cdot \left[\sqrt{1229 + (614 \cdot \sin(\theta_{HS}))^2} - 614 \cdot \sin(\theta_{HS})\right] \tag{20}$$

where *amr* represents the air mass ratio. P_H is the pressure at the altitude of the airship, P_0 is the sea level pressure that has a reference value of 101330 Pa. As shown in Fig. 5, the formula of solar height angle θ_H, solar declination angle θ_D and solar hour angle θ_{hour} can be given by

$$\theta_H = \sin^{-1}(\sin(\theta_D)\sin(\phi) + \cos(\theta_D)\cos(\phi) \times \cos(\theta_{hour})) \tag{21}$$

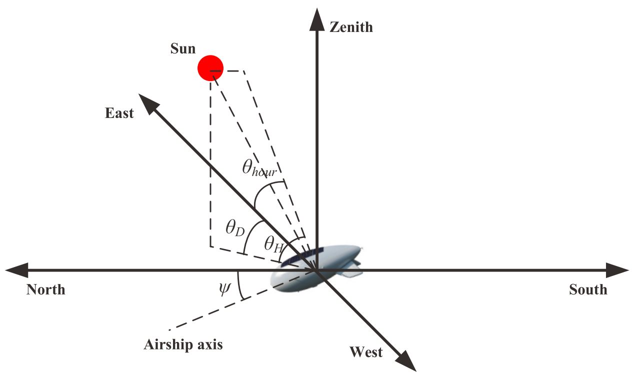

Fig. 5. Various angles of the solar irradiation.

$$\theta_D = [0.3723 + 23.2367 \cdot \sin(\theta_D) + 0.1149 \cdot \sin(2\theta_D) \\ -0.1712 \cdot \sin(3\theta_D) - 0.758 \cdot \cos(\theta_D) \\ +0.3656 \cdot \cos(2\theta_D) + 0.0201 \cdot \cos(3\theta_D)] \quad (22)$$

$$\theta_{hour} = 15 \cdot (t_n - 12) \cdot \pi/180 \quad (23)$$

where ϕ is the local latitude, t_n is accurate solar time, which can be defined by

$$t_n = t_s + e/60 + (\lambda - 120)/15 \quad (24)$$

where t_s is standard time, e is time difference, and λ is the local longitude. Time difference e is defined by

$$e = 9.87 \cdot \sin(2\theta_D) - 7.53 \cdot \cos(\theta_D) - 1.5 \cdot \sin(\theta_D) \quad (25)$$

The scattered radiation intensity I_S is defined by

$$I_S = \frac{0.5 \cdot I_0 \cdot \sin(\theta_d) \cdot amr(1 - \tau_h)}{amr - 1.31\tau_h} \quad (26)$$

The reflected radiation I_R is described by

$$I_R = r_{atm} \cdot I_D \quad (27)$$

where r_{atm} is the reflectivity that can be approximately adopted as 0.18 for a clear sky and 0.57 for overcast sky.

4.1.2. PV array model

The solar cell array on the upper surface of the airship is curved, and its curvature is consistent with the airship envelope shape (Tang et al., 2023). In order to establish an accurate radiation model, the finite element method is introduced. The entire PV array is divided into micro-elements, which can be regarded as planes, and the sum of all micro-elements receiving radiation is the radiation of the PV array. The airship surface governing equation can be expressed as

$$F = x^2 + z^2 - f^2(y) \qquad 0 \leqslant y \leqslant L \quad (28)$$

where L is the axial length of the PV array. The microelement area dA can be calculated with

$$dA = d\theta \cdot dy \cdot r \cdot \sqrt{1 + r\prime(x)^2} \quad (29)$$

where θ is the laying angle, and r is the radius of the corresponding circular section. The average vector of the micro-element in the body coordinate system can be given by

$$\begin{aligned} \boldsymbol{n}_{ij} &= (n_{ijx}, n_{ijy}, n_{ijz}) \\ &= \left(\tfrac{\partial F}{\partial x}, \tfrac{\partial F}{\partial y}, \tfrac{\partial F}{\partial z}\right) \Big/ \sqrt{\left(\tfrac{\partial F}{\partial x}\right)^2 + \left(\tfrac{\partial F}{\partial y}\right)^2 + \left(\tfrac{\partial F}{\partial z}\right)^2} \end{aligned} \quad (30)$$

Transformation matrix from body coordinate system to inertial coordinate system can be given by

$$\boldsymbol{R} = \begin{bmatrix} C_\theta C_\psi & S_\theta C_\psi S_\phi - S_\psi C_\phi & S_\theta C_\psi C_\phi + S_\psi S_\phi \\ C_\theta S_\psi & S_\theta S_\psi S_\phi + C_\psi C_\phi & S_\theta S_\psi C_\phi - C_\psi S_\phi \\ -S_\theta & C_\theta S_\phi & C_\theta C_\phi \end{bmatrix} \quad (31)$$

where ϕ , θ , and ψ are the roll angle, pitch angle, and yaw angle in the body coordinate system (Sun et al., 2015). The microelement average vector in the body coordinate system and the irradiation vector in the inertial frame $\boldsymbol{n}_s$ can be expressed as

$$(n_{ijIx}, n_{ijIy}, n_{ijIz})^T = \boldsymbol{R} \cdot (n_{ijx}, n_{ijy}, n_{ijz})^T \quad (32)$$

$$\boldsymbol{n}_s = (-\cos\theta_H \cdot \cos\theta_D, -\cos\theta_H \cdot \sin\theta_D, -\sin\theta_H) \quad (33)$$

The angle between the irradiation vector and the microelement normal vector can be expressed as (Dai et al., 2012)

$$\alpha_{ij} = \cos^{-1}\left(\frac{\boldsymbol{n}_{ijI} \cdot \boldsymbol{n}_s}{|\boldsymbol{n}_{ijI}| \cdot |\boldsymbol{n}_s|}\right) \quad (34)$$

As shown in Fig. 6, when the angle between the irradiation vector and the microelement normal vector is obtuse, the radiation intensity of the microelement is the absolute value of the dot product of the two; when the angle is acute, the irradiance value of the microelement is 0. The intensity of direct radiation I_{ij0} and scattered radiation of microelements I_{ijh} can be expressed as

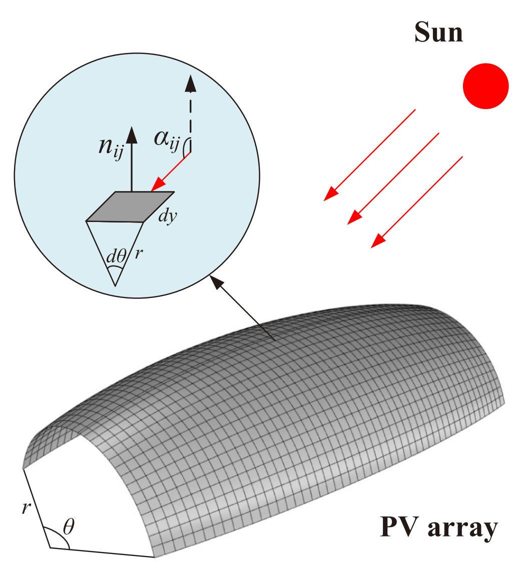

Fig. 6. Finite element model of the PV array.

$$I_{D,ij} = \begin{cases} 0 & 0 \leqslant \alpha_{ij} < \frac{\pi}{2} \\ |\boldsymbol{n}_{ijI} \cdot \boldsymbol{n}_s| \cdot I_{d0} & \frac{\pi}{2} \leqslant \alpha_{ij} < \pi \end{cases} \tag{35}$$

$$I_{S,ij} = \frac{1}{2} \cdot I_S \cdot \left(1 - \frac{n_{ijz}}{|\boldsymbol{n}_{ijI}|}\right) \tag{36}$$

The irradiation power of the microelement can be given by

$$P_{ij} = (I_{D,ij} + I_{S,ij}) \cdot dA_{ij} \tag{37}$$

The power generated by the battery array can be expressed as

$$P_{PV} = \sum_{i=1} \sum_{j=1} \eta_{ij} P_{ij} \tag{38}$$

where η is the conversion efficiency of PV array, which is related to capsule temperature of the airship,

$$\eta_{ij} = 0.2 - 0.0007 \cdot (T_{env} - 250) \tag{39}$$

4.2. Thermal model

The temperature of the airship affects the internal pressure of the capsule. The temperature difference between day and night in the flying environment of the stratospheric airship is huge. Therefore, in order to maintain the shape of the capsule at night, it is necessary to keep the air pressure high, but experiments show that capsule will be heated in the daytime and result in an increase of the air pressure, which will cause irreversible damage to the capsule material. Therefore, controlling the gas temperature inside the capsule has a great impact on the endurance of the airship. One of the most important ways is to speed up the airship in order to accelerate the heat transfer, which is closely related to the airship trajectory planning.

The gas temperature inside the capsule is only related to the envelope temperature, and the rise and fall of the temperature of the gas and the envelope are generally the same. To simplify the calculation, the following assumption is made:

Assumption 4.1. the temperature difference between the internal gas and the envelope can be ignored, thus the temperature of internal gas can be replaced by envelope.

In the calculation of solar radiation to the envelope, Because the projected area of the sun on the skin is related to the solar radiation angle, in order to simplify the calculation, the following assumptions is made:

Assumption 4.2. the envelope area is set to a constant value S_{ref}, which is the ground projection area of the airship.

If the surface area of the airship is S_{env}, S_{ref} can be expressed as

$$S_{ref} = \frac{1}{4} \cdot S_{env} \tag{40}$$

The thermal control equation of the airship envelope with conservation of energy is

$$m_{env} c_{env} \frac{dT_{env}}{dt} = Q_{sun} + Q_{out} \tag{41}$$

where subscript "env" represents the envelope. On the right side of the equation, Q_{sun} is solar energy input, and Q_{out} means the convective heat transfer from the envelope to the external environment.

The solar radiation received by the airship is composed of three parts, namely, direct $Q_{sun,D}$, scattering $Q_{sun,s}$, and reflection$Q_{sun,R}$,

$$Q_{sun} = Q_{sun,D} + Q_{sun,S} + Q_{sun,R} \tag{42}$$

The direct sunlight received by the airship is

$$Q_{sun,D} = \alpha_e \cdot I_D \cdot A_{ref} \tag{43}$$

where α_e is the envelope absorptivity for direct radiation from the sun.

The solar light scattering received by the airship is as follows

$$Q_{sun,S} = \frac{1}{2} \cdot I_S \cdot S_{ref} \tag{44}$$

Ground and cloud reflection the airship receive is as follows

$$Q_{sun,R} = \frac{4}{3} \cdot I_R \cdot S_{ref} \tag{45}$$

The energy transferred from the external environment to the airship envelope is

$$Q_{out} = h_{out} \cdot (T_{air} - T_{env}) \cdot S_{env} \tag{46}$$

where the heat transfer coefficient h_{out} between the envelope and external environment is the same as the heat transfer coefficient between the PV array and external environment.

4.3. Propulsion power model

The airspeed of the airship is determined by the propulsion motor RPM, and the motor RPM is related to energy consumption. Propulsion system power P_{prop} can be given by

$$P_{prop} = F_T v_{airspeed} / (\eta_{prop} \eta_{mot}) \tag{47}$$

where η_{prop} is the propeller efficiency, and η_{mot} is the motor efficiency. The thrust generated by the propulsion system can be expressed as (Gao et al., 2013)

$$F_T = \frac{1}{2} \rho_{air} S_{ref} C_D V_{airspeed}^2 \tag{48}$$

where S_{ref} is the cross-sectional area at the maximum shaft diameter, C_D is the drag coefficient.

5. Result and discussion

5.1. Case study

To verify the station-keeping strategy, a mission scenario based on the existing airship model is established.

The mission requires keeping a station in an area for one day (24 h). The center point of the area is in Beijing (40 N, 116E), and the radius of the mission area is 100 km. The starting time is set to 19:00, at which time the battery of the airship is usually full of charge. The wind field used is the real wind field at the location on July 15–16, 2021, and the solar irradiation is also set according to the time and location. The basic parameters of the stratospheric airship are listed in Table 1.

The goal of optimization is to maximize the total energy, in other words, to minimize the total energy consumption. Therefore, the cost function for optimization can be expressed as

$$J = -\dot{E} = -(\dot{E}_{loc} + \dot{E}_{wind} + \dot{E}_{battery}) \tag{49}$$

The rate of change of energy storage battery can be expressed as

$$\dot{E}_{battery} = \sum_{i=1}^{m}\sum_{j=1}^{n}\eta_{ij}p_{ij} - P_{prop} - P_{avio} - P_{load} \tag{50}$$

where P_{avio} is the power of the avionics system, P_{load} is the power of the load system, both of which can be regarded as constants when conducting trajectory planning. $\sum_{i=1}^{m}\sum_{j=1}^{n}\eta_{ij}p_{ij}$ represents the output power of the airship's solar array, P_{prop} is the power consumed by the propulsion system, which is related to the airspeed $V_{airspeed}$ of the airship.

According to the requirements of the actual airship, it needs to meet the position constraints, the airship capsule temperature constraints, and the airship battery energy storage constraints.

In summary, the optimization problem can be expressed as.

$max\{J\}$ St. constraints:

$$\begin{cases} D < 100km \\ T_{env} < -30^{\circ}C \\ SOC > 0\% \\ SOC_{end} = 100\% \end{cases} \tag{51}$$

State quantity:

$$\boldsymbol{x} = [x, y, T_{env}, T_{array}, E_{battery}] \tag{52}$$

Control amount:

$$\boldsymbol{u} = [V_{airspeed}, \gamma] \tag{53}$$

Table 1
The airship parameters.

Parameter	Value	Parameter	Value
Length, m	220	Efficiency of solar cells (273 K)	0.2
Diameter, m	54	Battery energy density, Wh/kg	330
Envelope area, m^2	33000	Center angle of PV array, °	90
Volume, m^3	380000	Efficiency for motor	0.93
Ceiling altitude, m	20000	Efficiency for propeller	0.77
PV array area, m^2	2200	Battery capacity, kWh	700

where D is distance to the center of the mission area, SOC is the percentage of battery energy, SOC_{end} is the percentage of battery energy at the end time and γ is the yaw angle.

After an optimization cycle (24 h), the energy battery needs to be fully charged, so as to ensure the sustainability of the next flight. The optimized trajectory is shown in Fig. 7. The red circle is the mission area, the green line is the optimal trajectory, and the gray line is the potential trajectory of the algorithm attempt. The airship did not fly out of the mission area during the whole flight process. After an optimization cycle, the airship position is 57.98 km away from the center point. The airship's parameters during the cycle are shown in Fig. 8. The maximum temperature of the capsule is −34.18°C, the minimum SOC of the airship is 3.80%, and the final SOC is 100%, all of which meet the mission requirements.

This typical scenario demonstrates the ability of the RRT-SK strategy to resist the wind by flying upwind of an impending strong wind in advance to have more space to be forced to retreat when the strong wind arrives. Which direction is upwind and how long to fly upwind is automatically determined by the strategy. This feature ensures that the airship is still able to extend its station-keeping time in other wind scenarios, the generalization of which will be discussed in Section 5.3.

5.2. Comparison

There are two conventional station-keeping strategies, namely, target-oriented strategy and wind-oriented strategy. Similar to the RRT-SK strategy, the control amount is the airship's heading angle and airspeed, and then plan the trajectory. The following is a brief introduction:

(1) The target-oriented strategy makes the airship always head for the predetermined target point. Airship's heading angle will be determined by the relative position between the target point and the airship, and the airspeed is a fixed value determined by the energy constraint within an optimization cycle.

(2) The wind-oriented strategy takes into account the impact of the wind on the airship. The airship's heading angle is always facing the wind direction and keeps the airship flying against the wind. In this way, the relative ground displacement can be reduced as much as possible. The airspeed is set according to the solar radiation and usually adopts different airspeeds according to the local time. In the daytime with strong solar radiation, the airship has more energy and adopts a higher airspeed V_{Day}, with no solar cell charging at night, using a lower airspeed V_{Night}.

A comparison of the constraints considered in the airship trajectory planning strategies is shown in Table 2. Compared with the conventional strategy, the cost function of the RRT-SK strategy takes wind field, target, location constraints, and other constraints into account.

Compared with the conventional strategy, the optimization parameter potential energy of the RRT-SK strategy

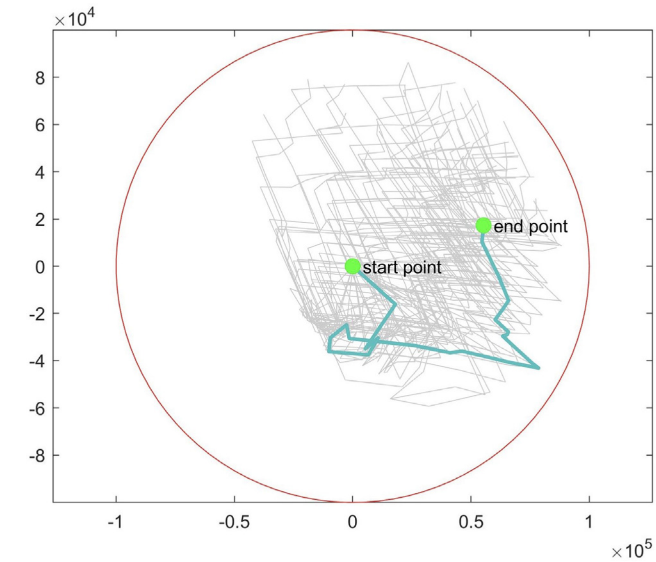

Fig. 7. Optimized trajectory generated by the RRT-SK.

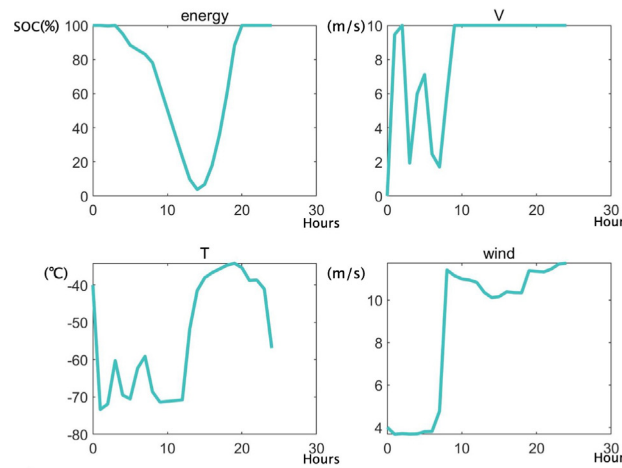

Fig. 8. Parameters of the airship during an optimization cycle.

includes wind field, target, location constraint, and other constraints.

For comparison, the target-oriented strategy and the wind-oriented strategy are employed on the same mission scenario as in Section 5.1. A simulation was raised to test the effectiveness of the three strategies on different dates in 2021. Station-keeping in the mission area for 24 h and meeting the constraints is considered a success day.

Fig. 9 shows the average wind speed of the mission area for one day in 2021. The results of the simulation are shown in Fig. 10, where navy blue represents the RRT-SK strategy, lake blue represents target-oriented strategy, and red represents wind-oriented strategy. It can be seen that success days are concentrated in the five months with low wind speeds, from April to September. If the average wind speed of the day exceeds the maximum airspeed of the airship, the airship's station will not be able to keep under any strategy. In the low wind speed months, the RRT-SK performs the best, with the number of success days all exceeding or equal to the wind-oriented strategy, and the target-oriented strategy performs the worst.

Taking June 16, 2021 as an example, the airship trajectory and status curves for 24 h under different strategies are shown in Fig. 11, Fig. 12. Under the three strategies, wind speed in the area of the airship is almost the same from 0 h to 10 h, at 6 h the RRT-SK does not choose to fly at high airspeed to resist the wind like other strategies, but reduces the airspeed to 0 and drifts with the wind, because the RRT-SK strategy regards the current wind direction as the direction of the total energy increase. After 24 h, the distance between the airship location and the center point of the area under the RRT-SK strategy is 56.34% and 44.33% better than the target-oriented strategy and wind-oriented strategy, respectively.

The trajectory followed by the RRT-SK strategy appears to be the longest, while the energy consumption is roughly the same for all three strategies, which is due to the different flight heading angles. Fig. 13 shows the wind field in the mission area, it can be seen that the wind speed at the beginning of the mission is a north wind of less than 5 m/s, then the wind speed gradually increases to 5–10 m/s, the wind direction changes between northwesterly and northeasterly, and finally at 18 h of the mission time the wind speed becomes stronger to over 10 m/s, which is beyond the range of the airship's ability to withstand, and at this time, the airship following the other two strategies other than RRT-SK will be blown out of the mission area. The RRT-SK does not waste energy to resist the east or west wind component in the early hours, and flies as far upwind as possible to resist the strong north wind afterward, the characteristic of long-time planning of the RRT-SK allows the airship to store the energy in the wind potential when the wind speed is small so that it will have more energy to resist the strong wind that came later.

Table 2
The constraints considered in the airship trajectory planning strategies.

Strategy	Wind field	Target	Location constraint	Other constraints
Target-oriented	×	○	×	×
Wind-oriented	○	×	×	×
RRT-SK	○	○	○	○

5.3. Universality analysis

According to Section 5.1, the RRT-SK strategy has advantages in this scenario, but its universality cannot be proved. This chapter will discuss the applicability of the algorithm when the mission scenario changes, such as the wind field, position constraints, energy constraints, and the airship capabilities change.

5.3.1. Impact of wind field change

When the wind field changes, the potential energy of the wind field will change accordingly. If the airship always

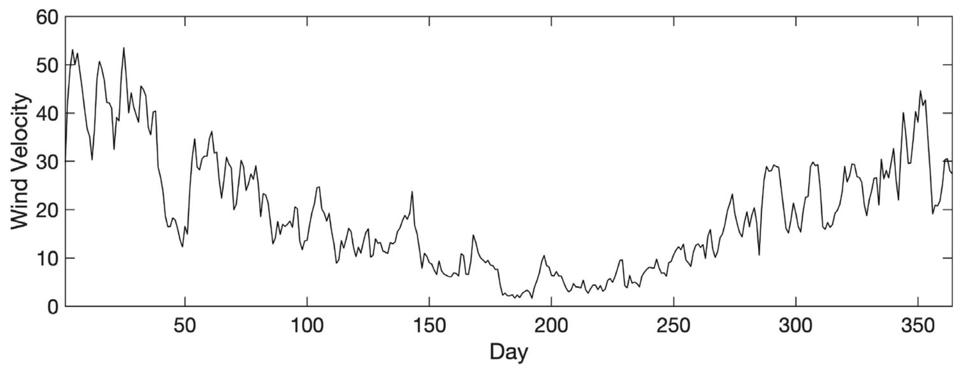

Fig. 9. The average wind speed of the mission area for one day.

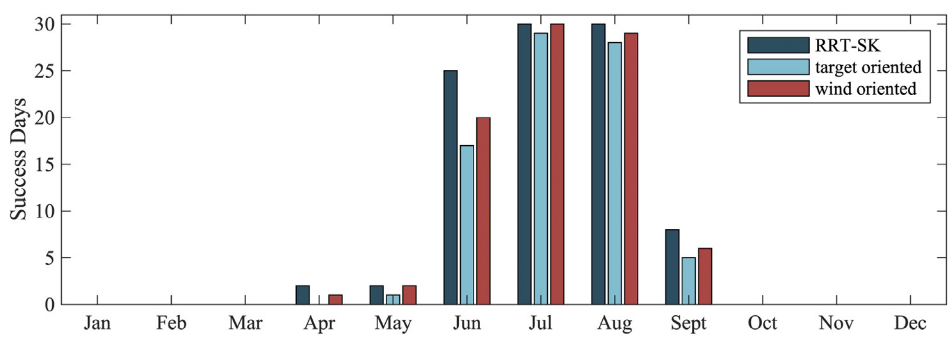

Fig. 10. Success days in 2021.

flies to the upwind area, the airship will be in a disadvantageous position if the wind direction changes. This problem can be avoided by the random characteristic of the RRT-SK. After the flight begins, the RRT-SK will extend the potential flight path in all directions, ensuring the optimization of the algorithm. Therefore, the RRT-SK can cope well with the impact of wind.

Fig. 14 shows the success rates of the three strategies at different wind speeds and mission area radii. The success rates of all three strategies remain high at a wind speed below 8 m/s, with wind speed increases, the difficulty of the station-keeping mission increases. The success rate of the RRT-SK strategy remains ahead at different wind velocities, and maintains a chance of success when the wind speed exceeds the wind resistance of the other two strategies, e.g., at the radius of 50 km with a wind speed of 9–10 m/s, at the radius of 100 km with a wind speed of 10–11 m/s, and at the radius of 200 km with a wind speed >11 m/s.

5.3.2. Impact of position constraints

The change of mission area directly affects the wind resistance of the airship, and the RRT-SK is the least sensitive to the change of area radius compared to the conventional strategy, which is determined by the energy storage characteristics of the RRT-SK wind field. For example, when the mission area radius is small, a short period of strong winds will cause the airship to fly out of the area

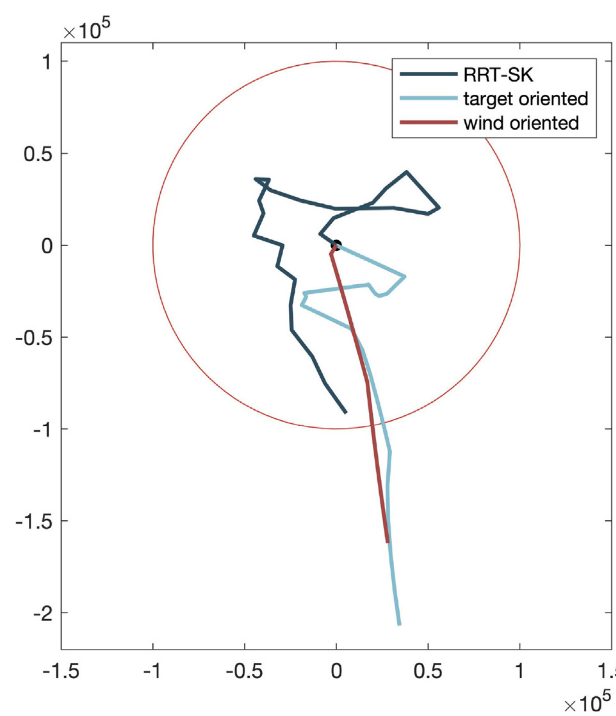

Fig. 11. Comparison of trajectories generated by different strategies.

and lead to mission failure, and if the mission area increases, the airship can resist the strong winds for a longer time. Fig. 14 shows the mission success rate under

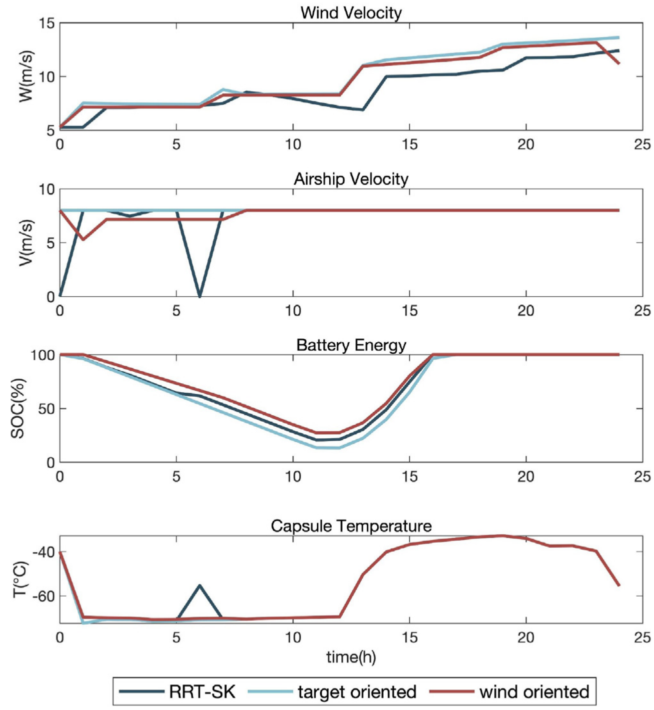

Fig. 12. Comparison of flight parameters under different strategies.

different mission radii R. As the mission radius decreases from 200 km to 100 km, the success rate of target-oriented strategy under 8–9 m/s wind speed decreases significantly, and the success rate of all three strategies under 9–10 m/s wind speed decreases, and the reduced success rate is the RRT-SK>wind-oriented>target-oriented = 0. When the mission radius is reduced to 50 km, only the RRT-SK maintains a certain success rate at 9–10 m/s wind speed. The RRT-SK uses the properties of the wind field potential energy to keep the airship in the upwind region. When the wind speed increases, the airship can retreat a longer distance without flying out of the mission area, and therefore can withstand stronger winds for a longer time.

5.3.3. Long time validation

The mission time of the cases shown in 5.1 is one day, and although it directly reflects the superiority of the

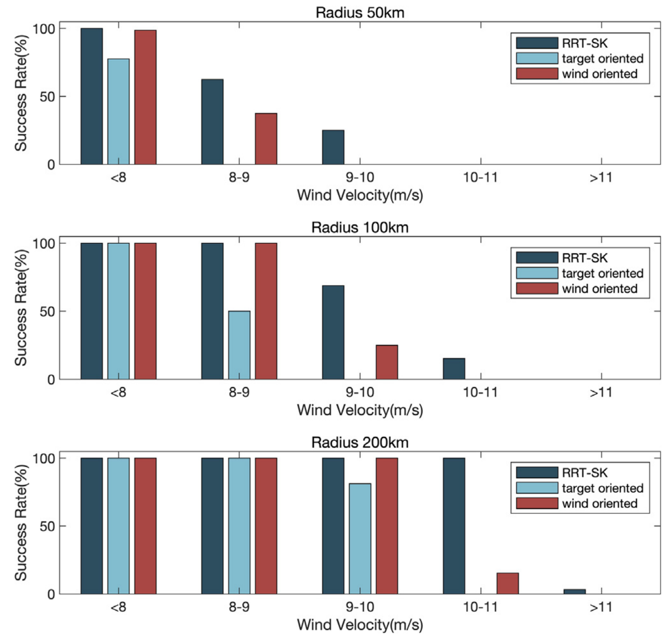

Fig. 14. The success rates at different wind speeds and mission area radii.

RRT-SK strategy in resisting strong winds, the actual use of the region resides often for several weeks, and the effect of the strategy used for a long time needs to be validated. Compared to one day mission, the starting position of the day after when running for a long time will be the same as the position at the end of the previous day, and the position will be inherited. Since the one-day missions under all three strategies were successful on the dates after September 18th (see Fig. 15), the starting time of the simulation is chosen as 19:00 on September 18th, the mission area radius is 100 km, and the wind field is the same as the actual wind field in 5.1. The results in Fig. 16 show that the RRT-SK strategy flew for 508 h until October 8, while the target-oriented strategy and the wind-oriented strategy flew for 324 h and 320 h, respectively, and flew out of the mission area on September 31. The station-keeping time of the RRT-SK strategy exceeds the conventional strategy by at least 56.79% in long-time simulation.

In contrast to the single-day simulation, the target-oriented and wind-oriented strategies also failed to survive the strong winds on September 31, while the RRT-SK

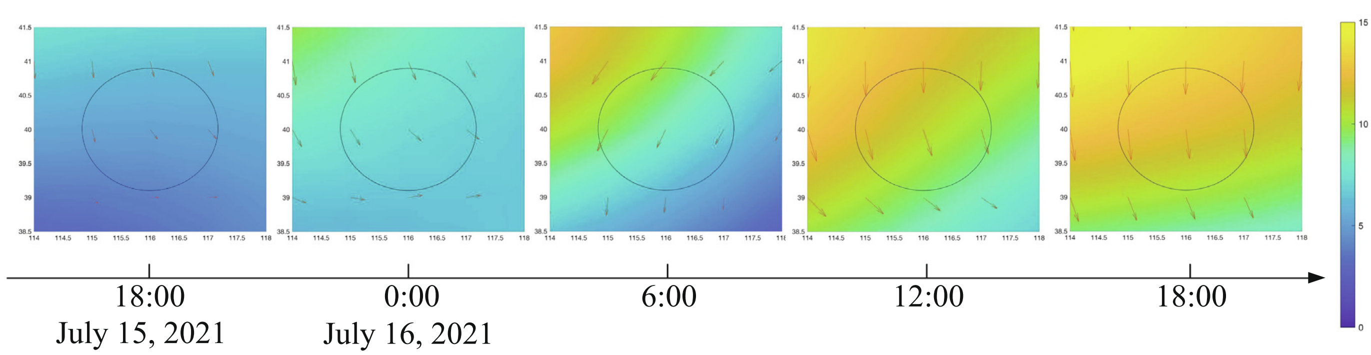

Fig. 13. Wind field in the mission area.

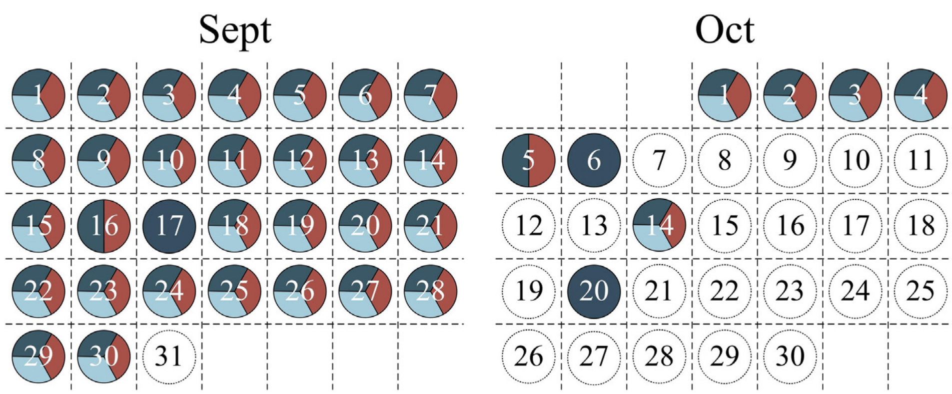

Fig. 15. Calendar chart indicating the one-day mission success days.

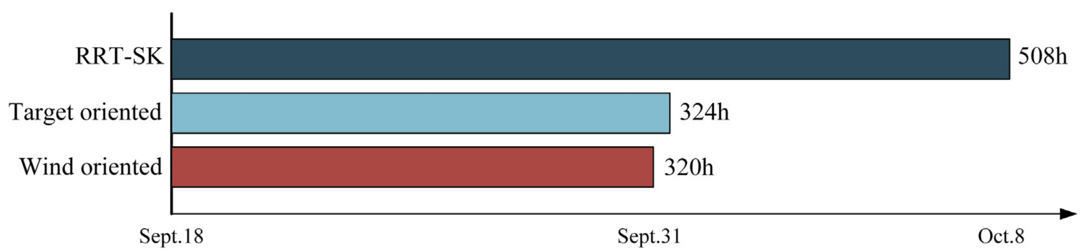

Fig. 16. Comparison of flight parameters under different strategies.

obtained a better upwind location on September 31 compared to the single-day simulation, ensuring that it remained within the mission area despite the strong winds. Moreover, the airship under the RRT-SK remained within the mission area for 2 days after October 6, which was not achieved by the single-day simulation. The results show that the RRT-SK has significant advantages in actual long-duration use.

6. Conclusions

In this article, a mission scenario of the stratospheric airship regional residence is proposed and analyzed. We proposed the RRT-SK strategy, a strategy for the existing multi-constraints station-keeping mission, which is based on rapidly exploring random trees algorithm and artificial potential fields. Moreover, a multidisciplinary model for the stratospheric airship was built and a case study of the RRT-SK was conducted and compared with other conventional strategies. The results fully prove the superiority of our strategy. And the universality discussion suggests that the RRT-SK strategy is applicable when mission scenarios change. There still remain some challenges, such as changes in the airship altitude due to sudden vertical winds, and trajectory planning with the limited airship control performance. In future work, we will consider the impact of 3D wind fields and introduce dynamic modeling in trajectory planning to enhance the usability of the strategy in reality.

Declaration of competing interest

The authors declare that they have no known competing financial interests or personal relationships that could have appeared to influence the work reported in this paper.

Acknowledgments

This work was supported by the National Natural Science Foundation of China under Grants (No. 62173016 and No. 51775021) and the Fundamental Research Funds for the Central Universities (YWF-23-JC- 02, YWF-23-JC-04).

References

Aggarwal, S., Kumar, N., 2020. Path planning techniques for unmanned aerial vehicles: A review, solutions, and challenges. Comput. Commun. 149, 270–299.

Alam, M.I., Pasha, A.A., Jameel, A.G.A., et al., 2023. High altitude airship: A review of thermal analyses and design approaches. Arch. Comput. Methods Eng. 30 (3), 2289–2339.

An, H., Hu, J., Lou, P., 2021. Obstacle avoidance path planning based on improved apf and rrt. In: 2021 4th International Conference on Advanced Electronic Materials, Computers and Software Engineering (AEMCSE).

Bai, X., Wang, L., Hu, Y., et al., 2023. Optimal path planning method for imu system-level calibration based on improved dijkstra's algorithm. IEEE Access 11, 11364–11376.

Bellemare, M.G., Candido, S., Castro, P.S., et al., 2020. Autonomous navigation of stratospheric balloons using reinforcement learning. Nature 588 (7836), 77–82.

Colozza, A., Dolce, J., 2003. Initial feasibility assessment of a high altitude long endurance airship. Technical Report.

Dai, Q., Fang, X., Li, X., et al., 2012. Performance simulation of high altitude scientific balloons. Adv. Space Res. 49 (6), 1045–1052.

d'Oliveira, F.A., Melo, F.C.L.d., Devezas, T.C., 2016. High-altitude platforms—present situation and technology trends. J. Aerospace Technol. Manage. 8, 249–262.

Du, H., Lv, M., Li, J., et al., 2019a. Station-keeping performance analysis for high altitude balloon with altitude control system. Aerosp. Sci. Technol. 92, 644–652.

Du, H., Lv, M., Zhang, L., et al., 2019b. Energy management strategy design and station-keeping strategy optimization for high altitude balloon with altitude control system. Aerospace Sci. Technol. 93 (Oct.), 105342.1–105342.9.

Foster, J., Aglietti, G., 2010. The thermal environment encountered in space by a multifunctional solar array. Aerosp. Sci. Technol. 14 (3), 213–219.

Gao, X.-Z., Hou, Z.-X., Guo, Z., et al., 2013. The equivalence of gravitational potential and rechargeable battery for high-altitude long-endurance solar-powered aircraft on energy storage. Energy Convers. Manage. 76, 986–995.

Iqbal, M., 2012. An Introduction to Solar Radiation. Elsevier.

Jin, J., Zhang, Y., Zhou, Z., et al., 2023. Conflict-based search with d* lite algorithm for robot path planning in unknown dynamic environments. Comput. Electr. Eng. 105, 108473.

Karaman, S., Frazzoli, E., 2010. Optimal kinodynamic motion planning using incremental sampling-based methods. In: IEEE Conference on Decision & Control.

Khoury, G.A., 2012. Airship Technology, vol. 10. Cambridge University Press.

Kitamura, Y., Tanaka, T., Kishino, F. et al., 1995. 3-d path planning in a dynamic environment using an octree and an artificial potential field. In: Proceedings 1995 IEEE/RSJ International Conference on Intelligent Robots and Systems. Human Robot Interaction and Cooperative Robots, vol. 2, IEEE, pp. 474–481.

Kreith, F., Kreider, J.F., 1978. Principles of solar engineering.

LaValle, S.M. et al., 1998. Rapidly-exploring random trees: A new tool for path planning.

Liu, C., Ma, Y., Cao, C., et al., 2023. Ship route planning in the pirate area via hybrid probabilistic roadmap algorithm within the context of the maritime silk road. Ocean Coastal Manage. 238, 106585.

Mueller, J., Paluszek, M., Zhao, Y., 2004. Development of an aerodynamic model and control law design for a high altitude airship. In: AIAA 3rd Unmanned Unlimited Technical Conference, Workshop and Exhibit, p. (p. 6479)..

Ou, J., Hong, S.H., Wang, Y., 2023. Adaptive visibility graph initialization on edge computing to accelerate hybrid path planning for mobile robots. In: SoutheastCon 2023, IEEE, pp. 411–417.

Shan, C., Lv, M., Sun, K., et al., 2020. Analysis of energy system configuration and energy balance for stratospheric airship based on position energy storage strategy. Aerosp. Sci. Technol. 101, 105844.

Sigurd, K., How, J., 2003. Uav trajectory design using total field collision avoidance. In: AIAA Guidance, Navigation, and Control Conference and Exhibit, p. 5728.

Souissi, O., Benatitallah, R., Duvivier, D., et al., 2013. Path planning: A 2013 survey. In: Proceedings of 2013 International Conference on Industrial Engineering and Systems Management (IESM), pp. 1–8.

Sun, K., Yang, Q., Yang, Y., et al., 2015. Numerical simulation and thermal analysis of stratospheric airship. Proc. Eng. 99, 763–772.

Tang, J., Xie, W., Zhou, P., et al., 2023. Multidisciplinary optimization and analysis of stratospheric airships powered by solar arrays. Aerospace 10 (1), 43.

Wang, J., Meng, X., Li, C., 2021. Recovery trajectory optimization of the solar-powered stratospheric airship for the station-keeping mission. Acta Astronaut. 178, 159–177.

Wang, X., Liu, Z., Liu, J., 2023. Mobile robot path planning based on an improved a* algorithm. In: International Conference on Computer Graphics, Artificial Intelligence, and Data Processing (ICCAID 2022), vol. 12604, SPIE, pp. 1093–1098.

Zhang, L., Li, J., Jiang, Y., et al., 2020. Stratospheric airship endurance strategy analysis based on energy optimization. Aerosp. Sci. Technol. 100, 105794.

Zhang, Y.-F., Zhu, M., Chen, T. et al., 2022a. Region coverage control for multiple stratospheric airships with combined self-/event-triggered mechanism. Defence Technol.

Zhang, Z., He, R., Yang, K., 2022b. A bioinspired path planning approach for mobile robots based on improved sparrow search algorithm. Adv. Manuf. 10 (1), 114–130.

Zhao, P., Chang, Y., Wu, W., et al., 2023. Dynamic rrt: Fast feasible path planning in randomly distributed obstacle environments. J. Intell. Robotic Syst. 107 (4), 48.